Lestinen, Sami; Kilpeläinen, Simo; Kosonen, Risto; Jokisalo, Juha; Koskela, Hannu; Melikov, Arsen

Flow characteristics in occupied zone – An experimental study with symmetrically located thermal plumes and low-momentum diffuse ceiling air distribution

Published in:
Building and Environment

DOI:
10.1016/j.buildenv.2017.11.020

Published: 15/01/2018

Document Version
Peer-reviewed accepted author manuscript, also known as Final accepted manuscript or Post-print

Flow characteristics in occupied zone – an experimental study with symmetrically located thermal plumes and low-momentum diffuse ceiling air distribution

Sami Lestinen[1,*], Simo Kilpeläinen[1], Risto Kosonen[1], Juha Jokisalo[1], Hannu Koskela[2], Arsen Melikov[3]

[1] Aalto University, School of Engineering, Department of Mechanical Engineering, Sähkömiehentie 4, 02150 Espoo, Finland.

[2] Turku University of Applied Sciences, Lemminkäisenkatu 14-18 B, FI-20520 Turku, Finland.

[3] International Centre for Indoor Environment and Energy, DTU Civil Engineering, Technical University of Denmark, Nils Koppels Alle, Building 402, 2800 Lyngby, Denmark.

*corresponding author: sami.lestinen@aalto.fi

Abstract

Airflow interaction between thermal plumes and vertical air distribution may cause significant effects on airflow characteristics such as velocity and temperature fields, turbulence intensity and fluctuation frequency. The flow interaction creates a random flow motion, vortical structures and turbulent mixing that can further yield a draught discomfort in an occupied zone. The main objective was to investigate large-scale airflow patterns and fluctuations as a result of interaction of buoyancy flows and diffuse ceiling flow. Experiments were performed in a test room of 5.5 m (length) x 3.8 m (width) x 3.2 m (height) with symmetrical set-up of cylindrical heat sources that gave a thermal load of 40-80 W/floor-m^2. The ventilation air was supplied through a diffuse ceiling with 0.5% degree of perforation. The observations indicate that the mean air speed and the airflow fluctuation increase with thermal load. Furthermore, the results show that a range of length scales increases with thermal load and with mean air speed. The results indicate that it can be difficult to fulfill the standard air velocity criteria for highly occupied spaces, where the maximum allowable mean air velocity is relatively low, i.e. 0.15-0.20 m/s. This is because the buoyancy flows from heat sources accelerate locally the flow field.

Keywords: thermal plumes, vertical air distribution, airflow characteristics, buoyancy flows, airflow interaction, Fourier analysis

1 Introduction

A healthy, energy-efficient and comfortable indoor environment is the key objective of air distribution. In accordance with the European standard 13182:2002 (E) [1], the main characteristics of airflow patterns in occupied zone are usually in the range of 0.1-0.5 m/s for the mean air speed, 20-80% for the turbulence intensity, 0-1 Hz for the frequency of velocity fluctuations and 18-35°C for the temperature. However, the mean air speed is usually below 0.35 m/s and the temperature below 26°C in occupied zone. In field surveys, draught has been identified as one of the biggest problems in commercial buildings [2]. To maintain comfortable thermal conditions is especially challenging in the office buildings because of high cooling demand. In those cases, even when the whole body thermal sensation is neutral, the increased local heat loss due to high velocity and/or low temperature may cause a local discomfort due to draught. In addition, air distribution is difficult to control in occupied zone [3].

Turbulence is a chaotic and a random flow motion that involve a wide range of scales [4]-[6]. Turbulent kinetic energy grows up from the mean flow into the largest eddies from where the turbulent kinetic energy is further transferred to the smaller and still smaller eddies until the turbulent kinetic energy is dissipated into the heat. This process is usually fast. Thus, a transfer occurs within short distance. Turbulence improve transport of energy, but requires continuous supply of energy against the turbulent stresses [7]. In addition, turbulence increases flow disturbances and interaction between the vorticity and the velocity gradients. Consequently, turbulence may have a significant effect on airflow characteristics.

The risk of draught increases when the airflow temperature decreases and the mean velocity and the turbulence intensity increase. Earlier studies have shown that the energy spectrum is proportional to the mean velocity; the fluctuation energy increases when the mean velocity increases [8] - [10]. In addition, Fanger et al. [11] proposed that the turbulence intensity has a significant effect on the sensation of draught. In a subsequent study, Melikov et al. [12] showed that also temperature fluctuation increases draught sensation. Furthermore, the airflow direction and the flow fluctuation can also have a substantial effect on local thermal sensation, e.g. the rising natural convection flow may interact with downward supply airflow and hence reduce the cooling of skin [13], [14]. In this way, the discomfort due to draught at vertical downward airflows can be reduced. For draught sensation, the experiments have shown that individuals are more sensitive to the airflow variations with the equivalent frequency between 0.2-0.6 Hz than the other frequency levels if the average air velocity is higher than 0.1 m/s [15], [16].

The restriction of draught rate (*DR*) model in the European standard EN ISO 7730:2005 [17] is that the model includes only the terms for local air temperature and local air speed as well as for turbulence intensity. The model does not take into account e.g. the airflow direction and interactions that have been shown to affect the sensation of draught [18]. In addition, an uncertainty of measurements should be known in order to carry out the reliable assessment and validation. Melikov et al. [19] proposed that 5 % uncertainty of draught rate can be realistically achieved.

Natural convection flows seem to dominate in highly occupied indoor environments, if the momentum flow of air jets is small [20]. Nielsen [21] represented that the driving force for the airflow field depends on the Archimedes number, which describes a ratio between buoyancy and inertial forces. Furthermore, Kosonen et al. [22] showed that a heat source strength and a thermal load distribution have a significant effect on air velocity field in a room. Generally, thermal load distribution has been shown to have a remarkable effect on thermal conditions [23], [24] and airflow patterns [25], [26].

Kandzia [27] studied the transient flow behavior of large-scale flow structures under natural and forced convection with symmetrical set-up of thermal loads and air distribution. The author found that a low-momentum supply airflow and high internal thermal loads cause an unstable airflow structure in a room. When the supply air velocity was increased, the airflow structures had more stable and two-dimensional behavior. This indicates more unstable airflow characteristics with the buoyancy-driven flows than with the momentum-driven flows. In addition, Müller et al. [18] demonstrated a significance of airflow interaction in indoor environments. The authors emphasized remarkable effects on airflow characteristics, such as mean air speed, turbulence intensity, fluctuation frequency and airflow direction.

Fourier transform can be conducted to investigate indoor airflow field [5], [12], [28]. Recently, Cheng and Lin [29] showed a difference in energy spectrums with several air distribution methods. Zhang et al. [30] in turn emphasized that a power spectrum may reflect the amount of turbulent kinetic energy in the flow motion of turbulent thermal convection. In addition, Wang et al. [31] represented the turbulent scales in a cabin mock-up, i.e. in a highly occupied thermal environment. The authors found that a range of spatial scales are on the order of 0.1 m…8×10^{-4} m and the time-scales correspondingly 0.8 s…0.01 s that characterize vortices in mixing region under opposing jets. In an earlier study, Chen and Srebric [32] stated that the smallest spatial scales, i.e. the Kolmogorov length scales, can be around 0.001 m to 0.01 m for the most indoor airflows.

The diffuse ceiling ventilation is a vertical air distribution method in which the supply air is distributed evenly through the perforated suspended ceiling down to the occupied zone [21], [33], [34]. The method has been shown to produce rather promising results compared to other ventilation methods [35] - [38], e.g. the diffuse ceiling ventilation can cool down higher thermal loads without draught than other common methods [39], [40]. However, the cooling capacity reduces towards increasing room height [41]. Furthermore, the diffuse ceiling ventilation can act as a radiant cooling ceiling [42] when the supply airflow decreases the ceiling temperature.

The main objective of the current study was to investigate airflow conditions, air speed fluctuation and turbulence scales with increasing thermal loads in a case where low-momentum diffuse ceiling air distribution and thermal loads are installed symmetrically in a test room. The symmetrical set-up was chosen, because the evenly distributed thermal loads and air distribution offer a good opportunity to observe average effects on airflow field. The novelty of this study is the extended airflow characteristics with gradually increased thermal load in a simplified indoor environment.

2 Methods

2.1 Test room

The measurements were carried out in a test room (Fig. 1) of internal dimensions of 5.5 m (length) x 3.8 m (width) x 3.2 m (height). The test room was located inside a laboratory hall such that the outer environment was also stable. The thickness of the envelope wall element was 80 mm in which the U-value was 0.3 W/m^2,K. The vertical air distribution was introduced by discharging supply air through a diffused ceiling into the occupied zone. The depth of the suspended ceiling was 0.35 m. The suspended ceiling was made of perforated Ecophon Advantage A glass-wool-plate elements with the dimensions of 600x600x20 mm^3 [43]. The degree of the open area of the perforation was around 0.5%. The diameter of the supply air nozzles in the diffused ceiling was 14 mm. Two Ventiduct VSR duct-diffusers [44] were installed sequentially above the suspended ceiling. The combined duct diffuser of diameter 0.2 m extended the entire length of the upper chamber. The flow pattern was 180° upwards and the suspended ceiling was 5 cm below the duct. The main target was to select a diffuser that brings supply air equally into the upper chamber from where the static pressure difference forces the supply airflow evenly through the suspended ceiling down to the test room.

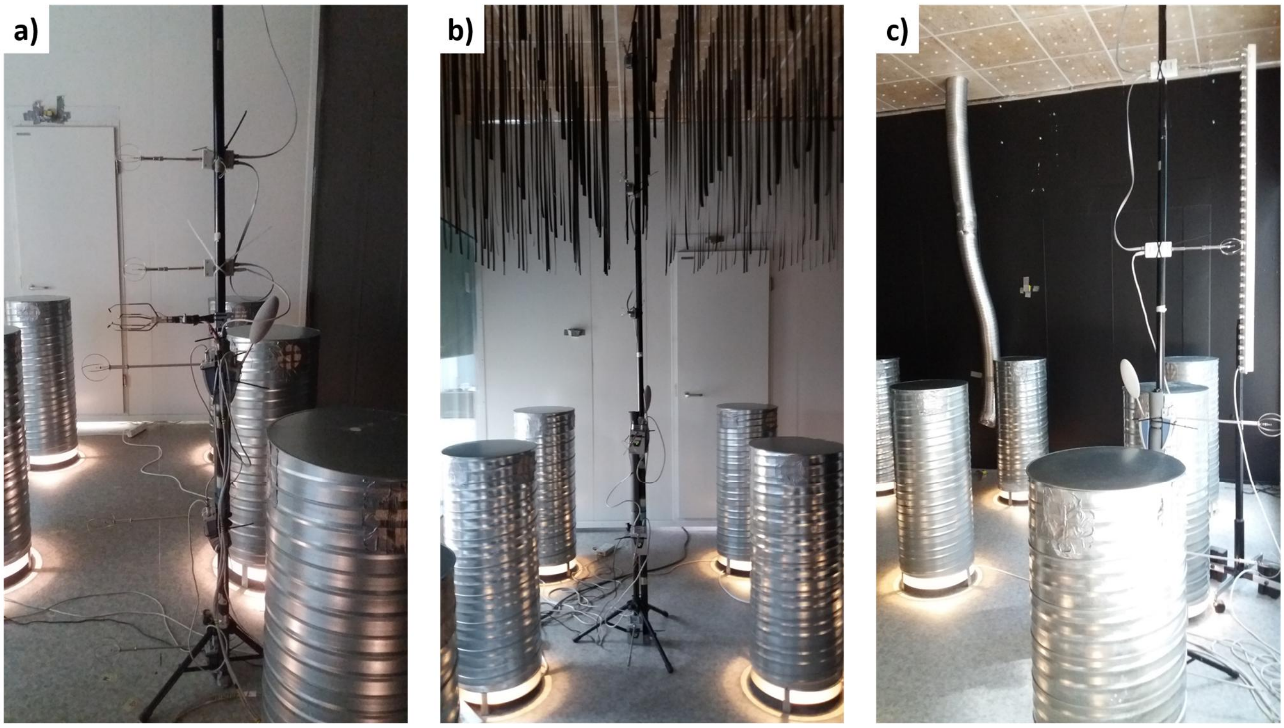

Fig. 1. Test room: a) cylindrical thermal loads and measuring mast with hot-sphere anemometers and ultrasonic anemometer, b) low-weight ribbons for detecting large-scale flow motions at the upper zone, c) exhaust air duct at the wall and led-light mast with equipment.

2.2 The experimental setup

The experimental setup was conducted by using 12 evenly distributed cylindrical heat sources of the diameter of 0.4 m [45] and the height of 1.1 m [46] including 0.1 m high legs against the vertical air distribution (Fig. 2). Thermal load was increased gradually such that internal heat load was 40-80 W/floor-m^2. On the contrary, the effect of supply air temperature was investigated with fixed thermal load as shown in Table 1. The flow field was measured using 7 hot-sphere anemometers. The detailed temperature differences of dummies and surrounding surfaces were observed with ThermaCAM P60 infrared camera [47]. The flow field was visualized with marker smoke that was video-recorded. The smoke visualization was done by releasing marker smoke into a supply air from the air-handling unit. In addition, a hand-released smoke was used for thermal plumes to detect air movement. The low-weight ribbons were used to detect large-scale eddies and flow motion in the upper zone before the actual measurements. The anemometers were installed into a measuring mast at the heights of 0.1 m, 0.6 m, 1.1 m, 1.7 m, 2.3 m and 2.9 m according to the European Standard EN ISO 7726:2001 [48]. Additional measurements were made at the height of 1.4 m.

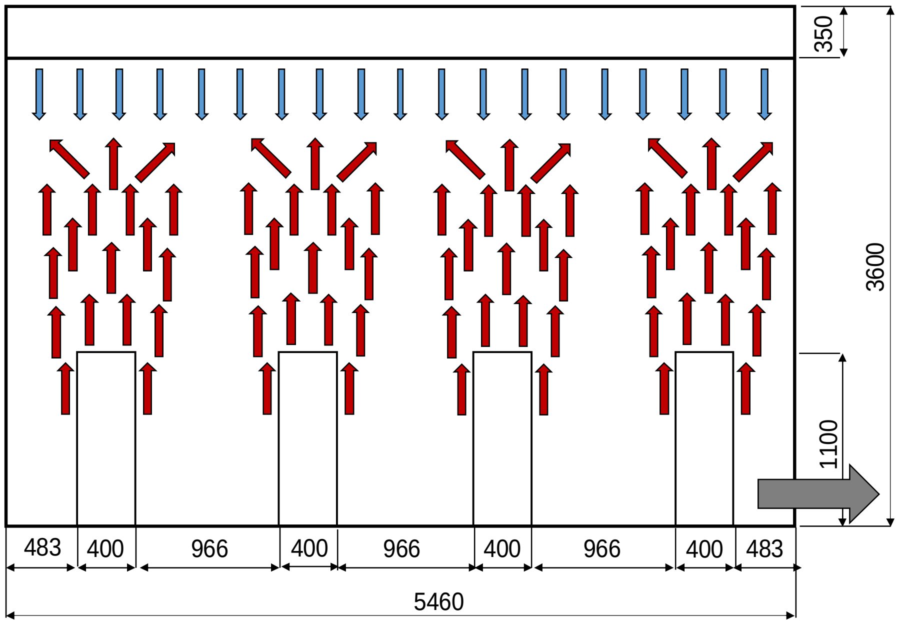

Fig. 2. A flow chart [mm] – thermal plumes (red arrows) and vertical air distribution (blue arrows). The supply air was distributed through a diffused ceiling and the exhaust air valve was installed at the height of 0.4 m from the floor (grey arrow).

Table 1. The test case parameters. The floor area is 21 m^2.

Test cases	**Case 1**	**Case 2**	**Case 3**	**Case 4**	**Case 5**	**Case 6**	**Case 7**	**Case 8**	**Case 9**
Heat load [W/m^2]	40±1	57±1	80±1	40±1	57±1	80±1	40±1	57±1	80±1
Supply air [l/s,m^2]	3.6±0.1	5.2±0.1	7.3±0.1	2.8±0.1	4.2±0.1	6.0±0.1	4.6±0.1	6.8±0.1	9.6±0.1
Supply air temp [°C]	17±0.3	17±0.3	17±0.3	15±0.3	15±0.3	15±0.3	19±0.3	19±0.3	19±0.3
Room temp [°C]	25-26	25-26	25-26	25-26	25-26	25-26	25-26	25-26	25-26

The measuring locations are shown in Fig. 3. The symmetrical set-up offered smaller investigation region, because the flow field was relatively similar in the test room. However, different locations can be classified as follows. The first group was the measuring locations between thermal loads in longitudinal direction, i.e. locations 3, 4, 7, 9. The second group was the locations between four thermal loads, i.e. locations 2, 8, 10. The third group was the locations between two thermal loads in wide-wise direction, i.e. locations 1 and 5. In addition, the thermal conditions were measured approximately 20 cm from the wall at the location 6. Those groups were classified, because the flow differences were expected in the occupied zone depending on the location of thermal loads. On the contrary, these locations were assumed to represent a reasonable sample of flow structures while investigating the averaged flow field.

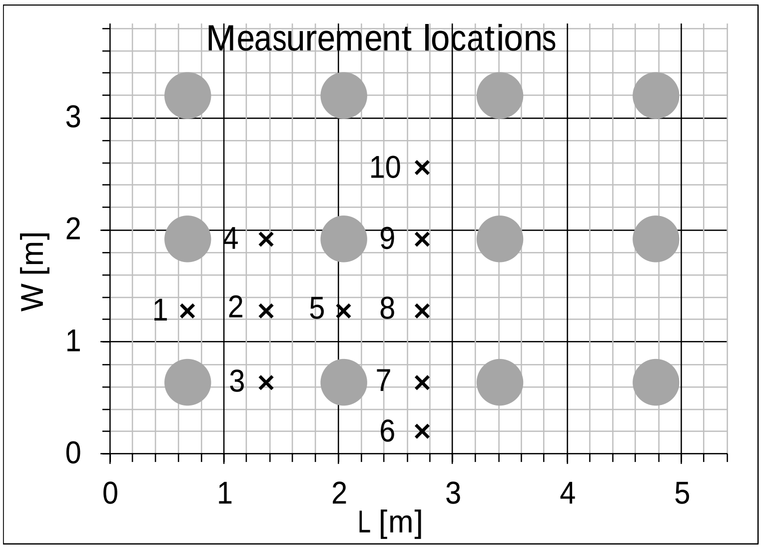

Fig. 3. The measurement locations 1-10 and the cylindrical heat sources (grey circles). The measured heights were at 0.1 m, 0.6 m, 1.1 m, 1.4 m, 1.7 m, 2.3 m and 2.9 m.

The three lowest sensors were the Vivo Draught 20T31 anemometers [49] and the four highest sensors were the wireless Sensoanemo 5100SF anemometers [50]. The readings were between 1 s and 2 s, respectively. This sampling rate enables observation for the most-energetic fluctuations up to 1 Hz and 0.5 Hz, respectively. However, the Fourier transform produces a spectrum up to 0.5 Hz and 0.25 Hz, because the spectrum is symmetric about a half of a sampling frequency [51], [52], i.e. the Nyqvist frequency. The measuring time-interval was 0.5 h. In addition, the Tinytagplus-2-meters [53] were attached on the internal and outer walls to observe near-wall temperature and humidity conditions. The supply and exhaust airflow rate was measured from the pressure difference of the IRIS-200 regulation and measuring device [54] by using the Swema 3000 measuring instrument [55]. The measurement and visualization equipment are summarized in Table 2.

Table 2. The measurement and visualization equipment.

Variable	***Meter-type***	**Model**	**Accuracy**
Temperature *Air speed* *Turbulence intensity*	Hot-sphere anemometer	Dantec dynamics Vivo Draught 20T31	Air speed (v): range 0.05-1.0 m/s ±0.01 m/s±0.025·v_{meas} Temperature (t): range 0-45°C ±0.15°C Sampling rate 10 Hz STDerr < 10 % upto 2 Hz, time-constant < 0.1 s (v) time-constant < 1 s (t)
Temperature *Air speed* *Turbulence intensity*	Hot-sphere anemometer	Sensor electronic SensoAnemo 5100SF	Air speed (v): Range 0.05-5 m/s ±0.02 m/s±0.015 v_{meas} Temperature (t): Range −10-50°C ±0.2°C Sampling rate 8 Hz STDerr<10 % upto 1.5 Hz 90 % response time < 0.2 s
Airflow patterns	Smoke visualization led light mast Video recorder low-weight ribbons	Opti-Mist Smoke generator and marker smoke	-
Temperature *Relative humidity*	Tinytag	Tinytagplus-2	-25…+85°C 0…100 % RH ±0.5°C (0…+45°C) ±0.8…0.5°C (-25…0°C) ±0.5…0.9°C (+45…+85°C) ±3.0 % RH at 25°C
Surface temperature	Infrared thermography	ThermaCAM™ P60 infrared camera	±2°C, ±2% of reading
Pressure	Measuring instrument	Swema 3000	±0.3 % read value, lowest ±0.3 Pa
Pressure difference	Regulation and measuring device	IRIS-200	±5 %

2.3 Airflow characteristics

The airflow can be characterized with common variables of fluid flow including the air speed, the temperature and their fluctuation. The fluctuation can be investigated by dividing the given variable into a time-averaged component and a fluctuating component as

$$\phi(x_i, t) = \bar{\phi}(x_i) + \phi'(x_i, t) \tag{1}$$

where ϕ is the variable, x refers to coordinate, t is the time, $\bar{\phi}$ is the time-averaged component and ϕ' is the fluctuating component of the variable, and subscript i denotes the index notation. In this way, the mean flow and the fluctuation phenomena can be separated. The time-averaged component in Eq. (1) is expressed as

$$\overline{\phi}(x_i) = \lim_{T \to \infty} \frac{1}{T} \int_0^T \phi(x_i, t)\, dt \tag{2}$$

where T is the averaging interval that should be sufficiently large compared to the fluctuating time-scale to describe the mean flow. Furthermore, the averaging of a discrete set of records N in a given location x_i can be expressed by the ensemble average as

$$\overline{\phi}(x_i, t) = \lim_{N \to \infty} \frac{1}{N} \sum_{n=1}^{N} \phi(x_i, t) \tag{3}$$

where $\overline{\phi}(x_i, t)$ is the ensemble-averaged component dependent on both the location x_i and time t, and N is the number of discrete values in the interval that average the fluctuations from the time-interval [56]. Consequently, the ensemble-averaged component is a sort of moving average of a certain time-interval while time is proceeding at a location x_i, whereas the time-averaged component in Eq. (2) is a mean value of a given time-interval at a location x_i.

In statistical mechanics, the cumulants may describe the expansion of distribution of continuous function or the discrete set of variable. The first cumulant is the mean value that describe an average of distribution. The second cumulant is the variance that describe a spread of distribution. The standard deviation is then a square root of variance. The deviation of sample can be calculated by using the sample standard deviation that can be written as

$$\phi_{\mathrm{SD}} = \sqrt{\frac{\sum_N \left(\phi_N - \overline{\phi}\right)^2}{N - 1}} \tag{4}$$

where the summation over the fluctuation component power of two is averaged and then equalized by taking a square root to quantify the amount of variation. The small standard deviation means small variation, thus the data set is near the mean value. The equivalent frequency (f_e) in turn is defined as a frequency of sinusoidal velocity fluctuations with the same ratio of the standard deviation of acceleration of velocity to the standard deviation of air velocity as in the random velocity fluctuations [16]. The equivalent frequency is defined as

$$f_e = \frac{1}{2\pi}\frac{\phi_{\mathrm{SDa}}}{\phi_{\mathrm{SDV}}} \tag{5}$$

where ϕ_{SDa} is the standard deviation of acceleration and ϕ_{SDV} is the standard deviation of air velocity. The characteristics of turbulent flow can be described e.g. by turbulence intensity, length scales, time scales and turbulent kinetic energy. The equivalent frequency is used together with turbulence intensity, mean velocity and air temperature to characterize sensation of draught [15]. The equivalent frequency decreases with decreasing fluctuation of forces and increases with decreasing fluctuation of air speed in the flow. At this stage, the forces that accelerates the flow presumably decrease slightly with lower thermal loads. However, also the air velocity fluctuation may decrease slightly. The ratio of those parameters comes from the statistical airflow conditions, sampling rate and measured time-interval.

Local thermal comfort is normally evaluated using draught rate index (*DR*). The Standard EN ISO 7730:2005 [17] defines the draught rate as

$$DR = (34 - t_{a,l})(\bar{u}_{a,l} - 0.05)^{0.62}(0.37 \cdot \bar{u}_{a,l} \cdot Tu + 3.14) \tag{6}$$

where $t_{a,l}$ is the local air temperature in degrees of Celsius from 20°C to 26°C, $\bar{u}_{a,l}$ is the local mean air velocity from 0.05 m/s to 0.5 m/s, and Tu is the local turbulence intensity in percent from 10% to 60%. The given draught rate model is based on the results from the human subject experiments [11]. It is limited to sedentary activity with a thermal sensation close to neutral. The sensation of draught is lower with higher activities than 1.2 met and for people feeling warmer than neutral. The turbulence intensity [17], [5], [57] can be defined as

$$Tu = \frac{u_{\mathrm{SD}}}{\bar{u}} \times 100 = \sqrt{\frac{2}{3}\frac{k_t}{\bar{u}^2}} \times 100 \tag{7}$$

where u_{SD} is the standard deviation of velocity in Eq. (4), $\bar{u}$ is the mean air speed in Eq. (2) and k_t is the turbulent kinetic energy. Turbulent kinetic energy can be determined as

$$k_t = \frac{1}{2}(\overline{u'u'} + \overline{v'v'} + \overline{w'w'}) \tag{8}$$

where u', v', w' denote the velocity fluctuation components in every coordinate direction in the flow. Hanzawa et al. [8] proposed that turbulent kinetic energy can be approximated as

$$k_t = \frac{1}{2}\overline{U'U'} \tag{9}$$

where U' is the fluctuation component of air speed when omnidirectional probe is used in measurement. This is equal to the turbulent kinetic energy taken from the isotropic turbulence conditions

$$k_t = \frac{3}{2}\overline{u'u'} \tag{10}$$

where u' is the fluctuating component such that $\overline{u'u'} = \overline{v'v'} = \overline{w'w'}$.

The Fourier transform of airflow fluctuation represents a frequency distribution from the set of discrete values of a given variable over the time-interval by providing the sinusoidal components of original function with certain frequency [58], [59]. The Fourier transform can be expressed as

$$\hat{\phi}(\omega) = \int_{-\infty}^{\infty} \phi(t)e^{-i\omega t}\, dt \tag{11}$$

where ω is the angular frequency and t is the time. The angular frequency can be determined as $\omega = 2\pi f$ and $f = 1/t$ where f is the frequency. The outcome of the Fourier transform is the complex-valued function $\hat{\phi}(\omega)$. The frequency distribution can then be presented in a real number set by taking the absolute value $|\hat{\phi}(\omega)|$ from the transformed function which shows the magnitude spectrum. Furthermore, the power spectrum is determined as $|\hat{\phi}(\omega)|^2$. The Fourier transform was calculated using Matlab R2016 and R2017 software [60], [61]. The Discrete Fourier transform is defined as

$$\hat{\phi}(f)_k = \sum_{j=1}^{N} \phi(t)_j e^{(-2\pi i(j-1)(k-1)/N)} \tag{12}$$

where *j* and *k* denotes the indexes and *N* is the sample of the discrete data set. The power spectral density describes the distribution of power as a function of frequency that provides a normalized power spectrum. The power spectral density was calculated using the Fast Fourier Transform (FFT) method that was based on the Discrete Fourier transform (DFT) method in Matlab software. Consequently, the power spectral density is determined as

$$S(f) = \frac{1}{N} \left|\hat{\phi}(f)\right|^2 \tag{13}$$

where the divisor *N* normalize the result. The energy spectrum can be expressed as

$$\int_0^\infty E(f)df = \overline{u_i^{'} u_i^{'}} \tag{14}$$

and it shows the density of distribution of velocity fluctuation in a range of frequencies, where $E(f)$ is the spectral distribution function of $\overline{u_i^{'} u_i^{'}}$. The fluctuation energy integral over the time can be determined from a numerical integral as

$$\mathrm{F}(E) = \int_{t1}^{t2} U'U' \, dt \approx \sum_{i=1}^{N} (U'U')_i \, \Delta t_i \tag{15}$$

Furthermore, the fluctuation energy ratio for a certain time-series records is determined as

$$\mathrm{X}(E) = \frac{\sum_{i=1}^{N} (U'U')_i \, \Delta t_i}{\sum_{i=1}^{N} (UU)_i \, \Delta t_i} \tag{16}$$

that in turn shows the relative amount of fluctuation energy compared with inertial energy including the mean airflow motions.

A wide range of scales characterize the turbulent flows, i.e. the largest scales are generally much greater than the smallest scales. The Kolmogorov scales [57], [62] represents the smallest scales which can be determined by using viscosity ν and dissipation ε as

$$v_\eta = (\nu\varepsilon)^{1/4} \; ; \; l_\eta = \left(\frac{\nu^3}{\varepsilon}\right)^{1/4} \; ; \; \tau_\eta = \left(\frac{\nu}{\varepsilon}\right)^{1/2} \tag{17}$$

where v_η is the velocity scale, l_η is the length scale and τ_η is the corresponding time scale. The integral scale l, on the other hand, describes the largest scales of motion [63] that can be expressed as

$$l = \frac{\bar{v}}{4}\frac{E(f)}{\overline{\overline{U'U'}}} \tag{18}$$

The integral scale is defined as a distance in which the fluctuating component remains correlated [56]. The largest length-scales may be on the order of a space height *H* in the test room. The time-scale was defined as a ratio of length scale to the mean air speed as

$$\tau_l \sim \frac{l}{\overline{\overline{U}}} \tag{19}$$

Therefore, the largest time-scales can be related to the low mean air speed levels and the largest length-scales. Generally, the largest time-scale was defined as a ratio of room height 3 m to the mean air speed at the certain location. Furthermore, the relationship between turbulent kinetic energy and dissipation can be approximated by Taylor [64]

$$\varepsilon \sim \frac{{k_t}^{3/2}}{l} \tag{20}$$

where the l reflects the largest length scales in the flow.

2.4 Uncertainty in measurement

The expanded uncertainty can be estimated for anemometers [19]. The uncertainty characterizes the dispersion of values in measurement [65]. Generally, the error in measurement is the difference between the recorded value and the true value which is unknown [5]. However, when all of the components of error have been evaluated, there still remains an uncertainty about the result [66]. The uncertainty consist of a random and a systematic uncertainty. The standard uncertainty does not have a probability associated with it, whereas the expanded uncertainty involve the probability. The uncertainty is estimated with statistical degree of confidence e.g. at the 95 % confidence and can be expressed as $\emptyset \pm d\emptyset$ for a given variable [67]. The accuracy of the hot-sphere anemometers (Table 2) on the air speed was $dU = \pm 0.01 \pm 0.025 \times U$ [m/s] in the seated person zone from the height of 0.1 m to 1.1 m that was mainly investigated. The valid air speed level was 0.05 m/s-1 m/s. This means that in decreasing air speed levels, the difference approaches to 0.05±0.011 m/s and the corresponding relative difference $\pm dU/U$ approaches to ±22.5 %. At the higher air speed levels, the given uncertainty approaches e.g. 0.4±0.02 m/s and ±5 %, respectively. Melikov et al. [19] proposed that the minimum realistic absolute expanded uncertainty at the 95 % confidence is $dU = \pm(0.025 + 0.025\overline{U})$ for the mean air speed and $dU_{std} = \pm(0.007 + 0.15U_{std})$ for the standard deviation as well as $dTu = \pm(4 + 0.23Tu)$ for the turbulence intensity. This means for the typical mean air speed levels correspondingly e.g. 0.1±0.028 m/s and ±28 % and 0.2±0.03 m/s and ±15 %, respectively. Consequently, the relative uncertainty increases towards lower air speed levels and dominate the uncertainty of functions on airflow characteristics.

3 Results

3.1 Supply air temperature

Fig. **4** shows the effect of supply air temperature on the statistics of mean air speed in the measured locations. Generally, the temperature level in the room was rather similar and no remarkable temperature stratification was found. Furthermore, the change in supply air temperature had only a small effect on the statistics of mean air speed, although the supply airflow rate was suited to target temperature below 26°C. Consequently, the relative difference of the mean air speed was below 3.3% with variable supply air temperature. However, the corresponding relative effect on standard deviation of given mean air speeds was below 5 %. Furthermore, the relative difference of standard deviation regarding with air speed records was below 1%. Therefore, the results are limited to the test cases 1-3 in which the supply air temperature was 17°C.

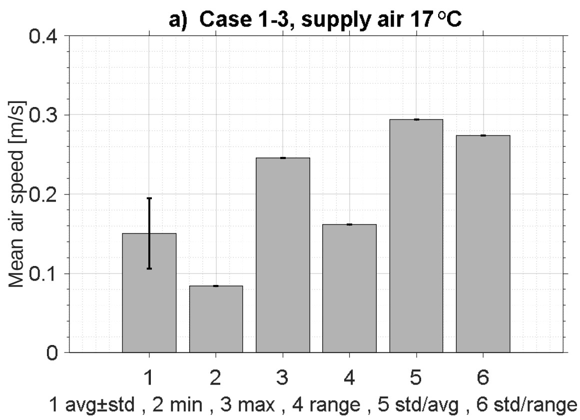

Fig. 4. The effect of supply air temperature on the statistics of mean air speed over each location below 1.1 m: a) supply air 17°C, b) supply air 15°C. Column 1 is the mean value of air speed ± standard deviation [m/s], Column 2 is the minimum, Column 3 is the maximum, Column 4 is the range of mean air speeds, Column 5 is the standard deviation over the mean value and Column 6 is the standard deviation over the range.

3.2 Mean air speed

Fig. 5 shows the average of mean air speeds in Eq. (2) as a function of room height and the corresponding mean air speed at the location 8 in the cases 1-3. The results show that the highest air speed level was observed near the floor at the height of 0.1 m and the lowest air speed level near the top of the heat sources at the height of 1.1 m. Therefore, also a vertical gradient of mean air speed was usually highest in this region.

Below the height of 1.1 m, i.e. a seated person zone, the average mean air speed was 0.12±0.03 m/s (±std) with a range of 0.08-0.18 m/s in the case of lowest thermal load level of

40 W/m². The average mean air speed increased by 47 % up to the highest thermal load level of 80 W/m². The standard deviation and range increased correspondingly by 38 % and 31 %, respectively. This indicates more deviation in the flow field with increasing thermal load.

At the height of 0.1 m, the mean air speed was greater, on average 0.20±0.03 m/s with the range of 0.13-0.25 m/s. Furthermore, the mean air speed reduced on average by 40 % up to the height of 1.1 m in which the mean air speed was lowest. The corresponding standard deviation and range decreased by 28 % and 18 %, respectively. This indicates more deviation with increasing mean air speed.

In the seated person zone, the uncertainty of measurements $dU = \pm(0.025 + 0.025\overline{U})$ [19] provided the mean air speed of 0.12±0.03 m/s and 0.18±0.03 m/s for the cases of 40 W/m² and 80 W/m², respectively. Hence, the relative uncertainty $dU/\overline{U}$ was ±23 % and ±17 % in those cases. The uncertainty of the standard deviation $dU_{std} = \pm(0.007 + 0.15U_{std})$ [19] of dataset records was correspondingly 0.062±0.016 m/s and 0.082±0.019 m/s. Thus, the relative uncertainty was ±27 % and ±24 %, respectively.

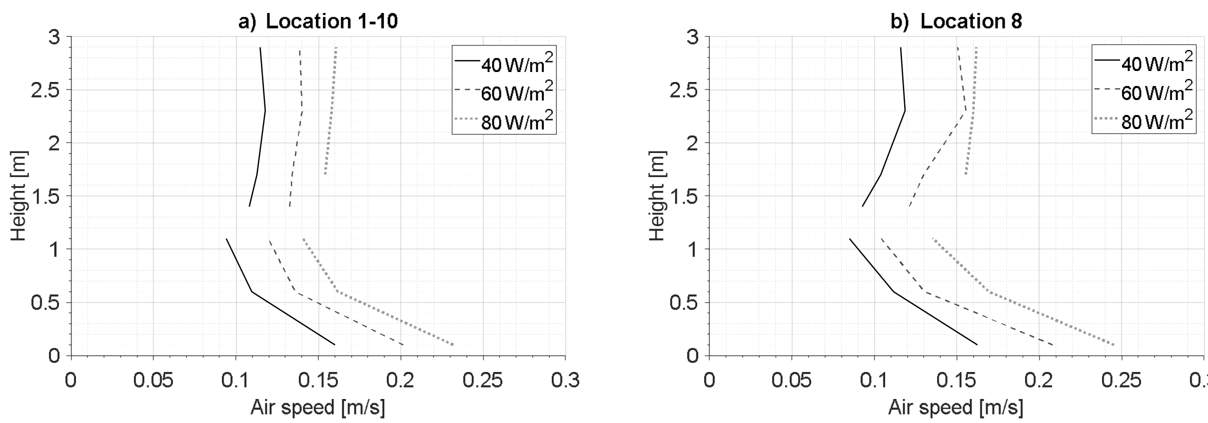

Fig. 5. a) the average mean air speed of the locations 1-10 and b) the mean air speed at the location 8 with thermal load levels of 40-80 W/m², cases 1-3 ($t_{,supply}$=17°C).

3.3 Turbulence intensity and draught rate

Fig. 6 shows that the lowest turbulence intensity in Eq. (7) was on average 40 % in the highest air speed region at the height of 0.1 m, and the highest turbulence intensity correspondingly 57 % in the lowest air speed region at the height of 1.1 m against the thermal load range. This is obvious because the turbulence intensity is a function of air velocity fluctuation and mean air speed, and the intensity typically increases towards lower air speed levels [18].

In the case of 40 W/m^2, the average turbulence intensity was 53±8 % (±std) with the range of 37 – 65 % in the occupied zone below the height of 1.1 m. The average turbulence intensity decreased only by 10% (relative difference) when the heat load increased from 40 W/m^2 to 80 W/m^2. This indicates that the thermal load had only a slight effect on turbulence intensity in the occupied zone.

At the height of 0.1 m, the average turbulence intensity was 40±5 % with the range of 31 – 57 %. The average turbulence intensity increased by 42 % from 0.1 m to 1.1 m. However, the corresponding standard deviation and the range decreased by 19 % and 40 %, respectively.

The uncertainty of measurements $dTu = \pm(4 + 0.23Tu)$ [19] provided the turbulence intensity of 53±16 % and 48±15 % in the cases of 40 W/m^2 and 80 W/m^2, respectively. It follows that the relative uncertainty of dTu/Tu was around ±31 % in both cases.

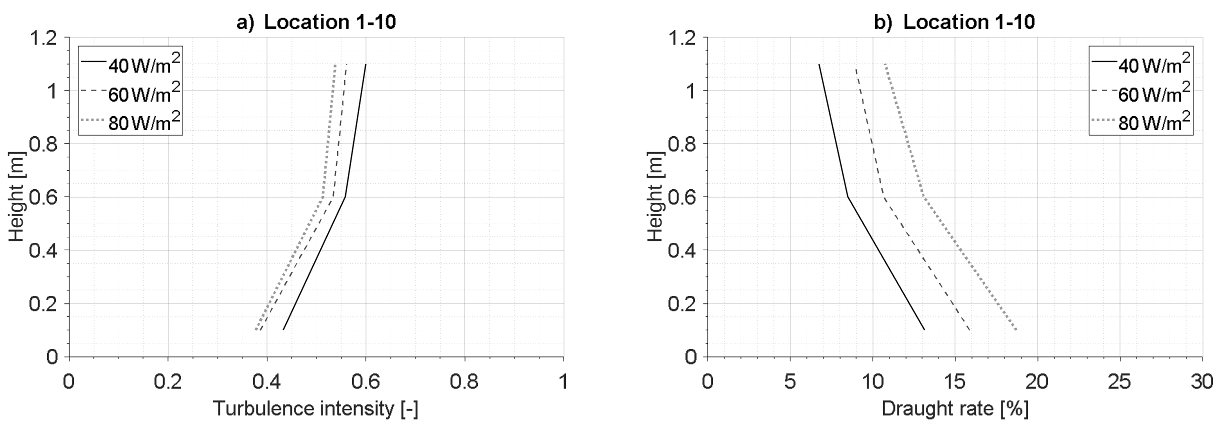

Fig. 6. a) the average turbulence intensity and b) the draught rate at the heights below 1.1 m with increasing thermal loads, case 1-3 (t_{supply}=17°C).

The local draught rate (DR) in Eq. (6) was on average 12 % in the occupied zone below 1.1 m. The minimum DR was 5.5 % and the range was around 15 % percentage points. The highest local draught rate were obtained at the height of 0.1 m, in which also the mean air speeds were the highest. On the other hand, the smallest local draught rates were observed at the height of 1.1 m where the mean air speeds were the lowest. The draught rate (DR) was at each location below 21 %. This indicates that the European Standard EN ISO 7730:2005 [17] would classify this thermal environment mainly at the category B (DR 10-20 %) with the prevailing mean air speed, the air temperature and the turbulence intensity levels. In addition, Melikov et al. [19] discussed that the measurements will produce below ±5% uncertainty to the draught rate with the given turbulence intensity and draught rate levels.

3.4 Airflow fluctuation

Fig. 7 shows the instantaneous air speed records at the height of 1.1 m in the location 8 with the mean air speed and the standard deviation range. In addition, the ensemble-averaged function over 60 sec interval represents the filtered deviation, because the slow fluctuation may have a periodical deviation. The mean air speed was 0.09±0.05 m/s in the case of 40 W/m^2, which increased by 60 % towards highest thermal load of 80 W/m^2. The corresponding standard deviation increased by 50 %. The increased standard deviation with higher thermal load describes a growing fluctuation that can have a significant effect on sense of draught and thermal comfort. In addition, the ensemble-averaged functions seem to have a certain periodicity between local extrema.

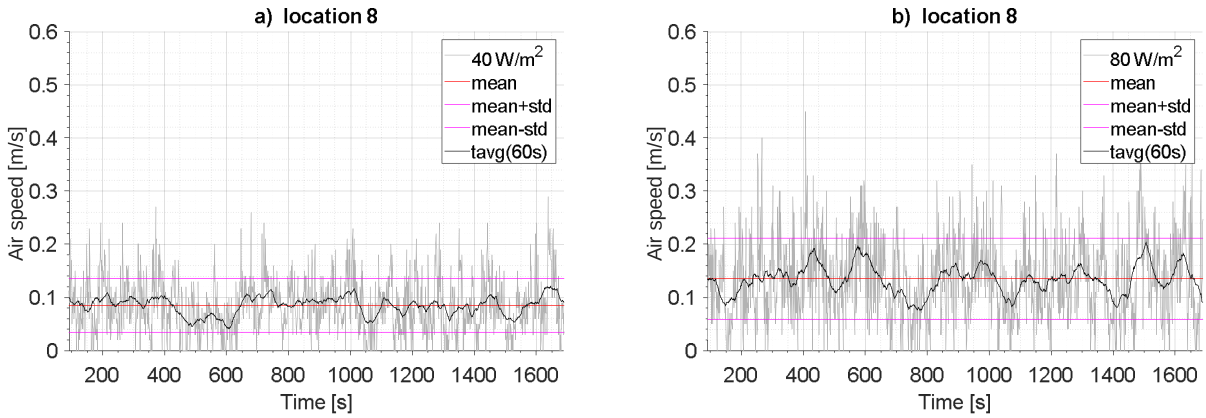

Fig. 7. The air speed fluctuation, the mean air speed, the standard deviation and the ensemble-averaged air speed over 60 s interval with the thermal loads of a) 40 W/m^2 and b) 80 W/m^2. Location 8 at the height of 1.1 m, case 1-3 (t_{supply}=17°C).

In the cases of 1-3, the equivalent frequency in Eq. (5) was generally between 0.10-0.18 Hz in the occupied zone below 1.1 m. In the case of 40 W/m^2, the equivalent frequency was on average 0.14 Hz over the measured locations. The equivalent frequency increased on average by 9 % from 40 W/m^2 to 80 W/m^2, thus the relative effect was at the same level than in turbulence intensity. The standard deviation and the range over the measured locations remained rather same level. In addition, the equivalent frequency increased on average only by 3.4 % from the height of 0.1 m up to the 1.1 m. However, the standard deviation and the range over the measurement locations reduced by 29 % and 39 %, thus significantly more than with thermal load, respectively. Overall, the results show that the equivalent frequency increased slightly with thermal load and with the height of the location.

3.5 Power spectral density

Fig. 8 shows the logarithmic presentation of power spectral density in Eq. (13) at the location 8. In the case of 40 W/m^2, the average power spectral density was $3.9\times10^{-3}\pm9\times10^{-4}$ m^2/s^2 (±std) over the measured locations in the occupied zone below 1.1 m. Consequently, the average fluctuation energy increased by 73 % from 40 W/m^2 to 80 W/m^2. The standard deviation increased similarly by 54 %. This also indicates increasing fluctuation with thermal load.

At the height of 0.1 m, the average power spectral density was $6.1\times10^{-3}\pm1.4\times10^{-3}$ m^2/s^2. The fluctuation energy decreased on average by 27 % from the height of 0.1 m up to 1.1 m. Hence, the fluctuation energy decreased towards lower mean air speed levels. However, the deviation and the range remained at the same level.

The mean power spectral density was non-linearly dependent on thermal load and any specific frequencies were not recognized. However, the ensemble-averaged functions were higher with higher thermal loads (Fig. **8**a). This indicates also an increased fluctuation energy with higher heat load. The normalized function by Etheridge and Sandberg [5], that is the ratio of the power spectral density over the variance, was at the same level with varying thermal loads (Fig. **8**b). Furthermore, the power spectral density decreased relatively gradually towards increasing frequency. The significant energy differences were recognized in the neighboring frequencies and in their multiplications while proceeding further the frequency axis. The highest power spectral density was in the mean flow at the zero frequency.

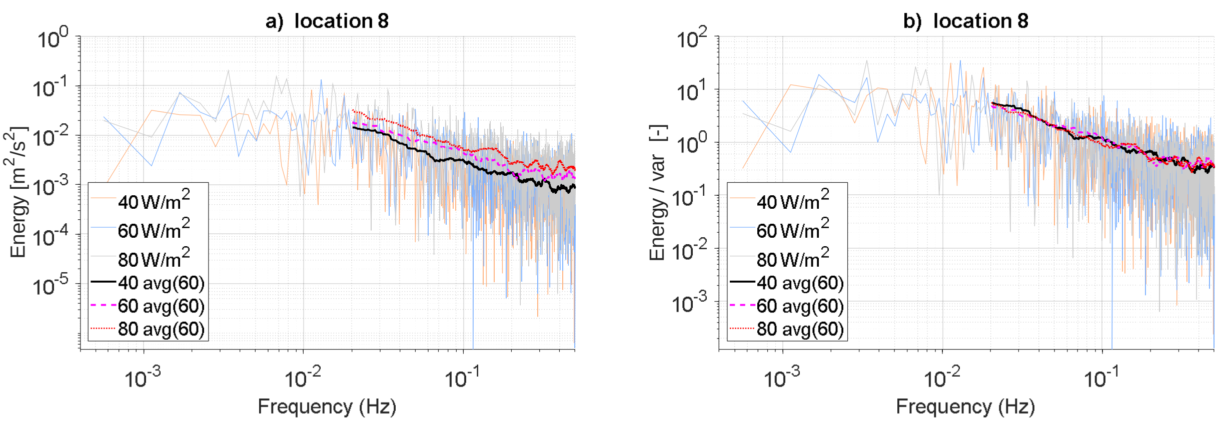

Fig. 8. The air speed fluctuation energy with thermal loads at the height of 1.1 m in the location 8, log-log scales: a) power spectral density, and b) normalized function by variance, case 1-3 (t_{supply}=17°C).

3.6 Fluctuation energy ratio

Fig. 9 shows the fluctuation energy integral in Eq. (15) and the corresponding fluctuation energy ratio in Eq. (16). In the case of 40 W/m^2, the fluctuation energy integral was on average 6.9±1.6 m^2/s below the height of 1.1 m. Furthermore, the corresponding fluctuation energy integral was 73% greater with 80 W/m^2 than with 40 W/m^2. This shows greatly the increase of fluctuation with thermal load. The fluctuation energy integral was greatest near the floor at the height of 0.1 m and decreased by 27% from 0.1 m up to 1.1 m, where the mean air speed was lowest. The fluctuation energy integral showed remarkable effects on flow field and characterize the airflow conditions under increasing thermal load circumstances.

The fluctuation energy ratio in Eq. (16) was on average 0.22±0.05 with the range of 0.12 – 0.30 in the case of 40 W/m^2 below 1.1 m. This indicates that the amount of airflow fluctuation was approximately 22 % of the airflow motions. The average ratio decreased by 16 % from 40 W/m^2 to 80 W/m^2. This implies that the ratio changes only slightly against the thermal load range. The fluctuation ratio was greatest at the height of 1.1 m in which the mean air speed was lowest. The ratio increased 76 % from 0.1 m up to 1.1 m. Hence, the relative difference was greater against the mean air speed range than against the thermal load range, conversely to that of the fluctuation energy integral.

Consequently, the results show that both the fluctuation energy integral and the energy integral including also the mean airflow motions increased with heat load and with mean air speed. However, their ratio, i.e. the fluctuation energy ratio decreased with increasing thermal load. This is apparent because the energy increase was greater in the total airflow motions than in the fluctuation airflow motions. This indicates actually that a relative portion of fluctuation energy increases while the thermal load and the mean air speed decrease, similarly than with turbulence intensity.

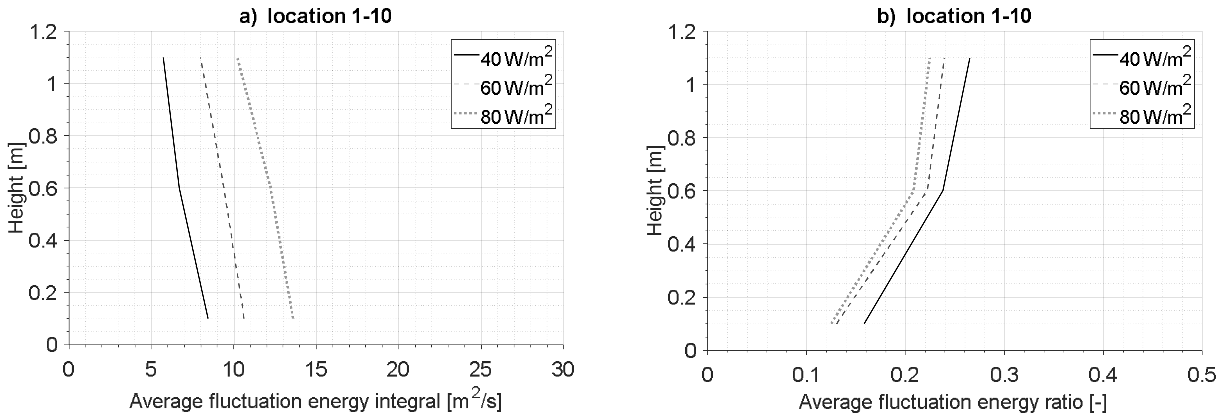

Fig. 9. a) The fluctuation energy integral and b) the fluctuation energy ratio against thermal loads below 1.1 m:, case 1-3 (t_{supply}=17°C).

3.7 Turbulent kinetic energy and turbulence dissipation

Fig. 10 shows the average turbulent kinetic energy in Eg. (9) and the turbulence dissipation in Eq. (20). The functions show that the given variables are greater with higher thermal load level and with higher mean air speed level.

The turbulent kinetic energy was on average $2.0 \times 10^{-3} \pm 4.5 \times 10^{-4}$ m^2/s^2 in the case of 40 W/m^2 below 1.1 m. The turbulent kinetic energy was on average 73 % higher with 80 W/m^2 than with 40 W/m^2, similarly than fluctuation energy integral. This indicates an increase with thermal load. However, the turbulent kinetic energy decreased on average by 27 % from 0.1 m up to 1.1 m, that was also similar than fluctuation energy integral. This shows relationship with those functions in Eq. (9) and Eq. (16), that is a fluctuation energy $f(U'U')$.

The turbulence dissipation, in turn, was on average $2.9 \times 10^{-5} \pm 1.0 \times 10^{-5}$ m^2/s^3 with 40 W/m^2 below 1.1 m. At this stage, the mean turbulence dissipation was even 127 % higher with 80 W/m^2 than with 40 W/m^2. Furthermore, the turbulence dissipation decreased on average by 36 % from 0.1 m up to 1.1 m. Hence, the effect of mean-air-speed range was smaller than the effect of thermal-load range in both variables.

The turbulence dissipation was smaller than the turbulent kinetic energy but it increased rather similarly with thermal load. However, the relative differences were greater in the turbulence dissipation than in the turbulent kinetic energy. Generally, the turbulence dissipation correlates also the turbulence production up-stream from the measured location, and therefore, the relative difference may differ from that in the turbulent kinetic energy. Turbulent kinetic energy reflects fluctuation and has thereby an effect on a sense of draught, and thermal comfort by increasing heat transfer between individuals and surroundings.

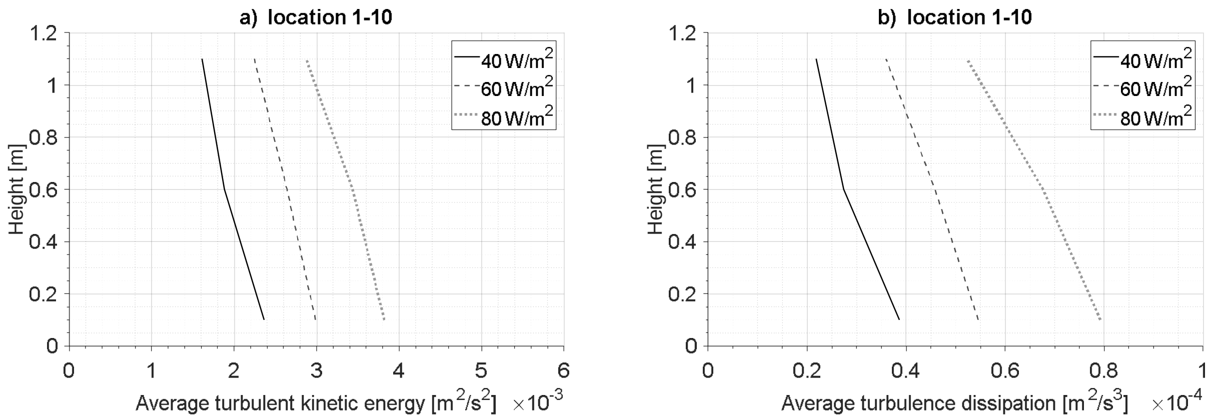

Fig. 10. a) The turbulent kinetic energy and b) the dissipation towards increasing thermal load below 1.1 m, case 1-3 (t_{supply}=17°C).

3.8 Length scales in the flow

Fig. 11 shows the integral scale in Eq. (18) and the Kolmogorov length scale in Eq. (17) as a function of room height. Generally, the integral scale was on average 1.4±0.9 m (±std) in the case of 40 W/m^2 and below 1.1 m. The integral scale increased on average by 16 % from 40 W/m^2 to 80 W/m^2, hence the integral scale increased slightly with thermal load.

At the height of 0.1 m, the integral scale was largest, i.e. on average 2.4±1.2 m over the thermal load range. Furthermore, the integral scale decreased on average by 63 % from 0.1 m up to 1.1 m. The relative differences show that the mean-air-speed range had a greater relative effect on the integral scale than that of the thermal-load range.

In the case of 40 W/m^2, the Kolmogorov scale was on average $3.5\times10^{-3}\pm3\times10^{-4}$ m over the measured locations below 1.1 m. Furthermore, the Kolmogorov scale was on average 19 % smaller with 80 W/m^2 than with 40 W/m^2. This depicts that the Kolmogorov scale decreases when thermal load increases, i.e. the smallest scales were inversely proportional to the thermal load. At the height of 0.1 m, the Kolmogorov scale was on average $2.9\times10^{-3}\pm3\times10^{-4}$ m over the thermal load range. In addition, the Kolmogorov scale increased on average by 14 % from 0.1 m up to 1.1 m, in which the mean air speed was lowest. At this stage, the mean-air-speed range had only a slightly smaller relative effect than the thermal-load range.

The result show that the smallest scales decrease towards increasing thermal load and the largest scales increase correspondingly, thus the range of length scales may increase with thermal load. Moreover, the largest scales were estimated near the floor that is logical, because the air speed level was highest in this region.

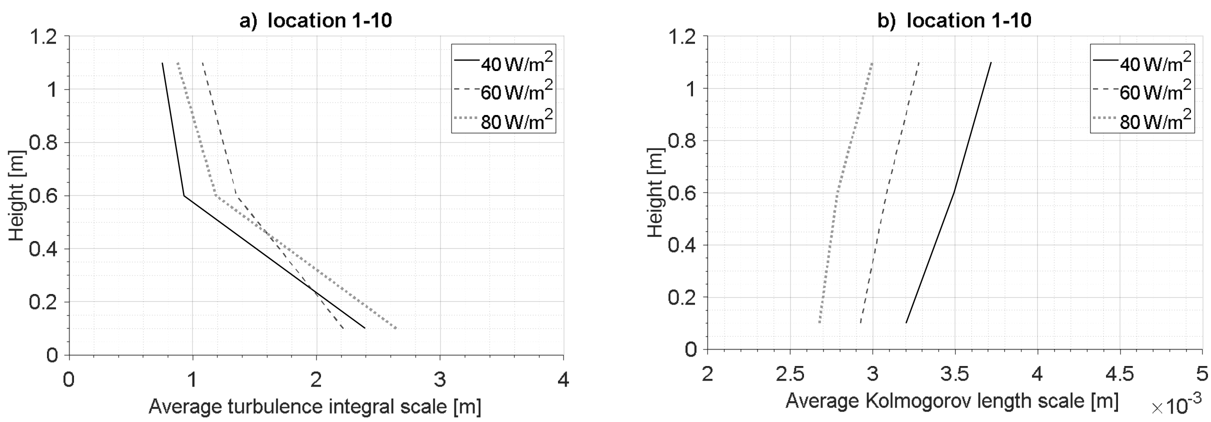

Fig. 11. The turbulence length scales towards increasing thermal loads at the occupied zone, case 1-3 (t_{supply}=17°C): a) large length scale, and b) small length scale.

3.9 Time scales in the flow

Fig. 12 shows the average time-scale of largest flow motion in Eq. (19) and the smallest scale flow motion in Eq. (17). The largest time-scales in the measured locations was on average 26±6 s (±std) in the case of 40 W/m^2 and below 1.1 m. The largest time-scale was on average 32 % smaller with 80 W/m^2 than with 40 W/m^2. At the height of 0.1 m, the corresponding time-scale was smallest, i.e. on average 16±3 s over the thermal load range. The largest time-scale increased on average by 69 % from 0.1 m up to 1.1 m where the mean air speed was low, because an eddy turn-over time increases when the velocity decreases.

The smallest time-scales, i.e. the Kolmogorov time-scale, was on average 0.8±0.1 s with 40 W/m^2 and below 1.1 m. The Kolmogorov time-scale was 34 % smaller with 80 W/m^2 than with 40 W/m^2, thus the relative effect was at the same level than in the largest time-scales. At the height of 0.1 m, the Kolmogorov time-scale was on average 0.5±0.1 s over the varying thermal loads. The Kolmogorov time-scale increased on average by 30 % from 0.1 m up to 1.1 m, thus the relative effect was smaller than in the largest scale.

It follows that the largest time scales were on the order of tens of seconds. Furthermore, those time-scales were decreasing towards increasing thermal load and mean air speed. This could affect sensation of draught and thermal comfort while the time-scales gets smaller.

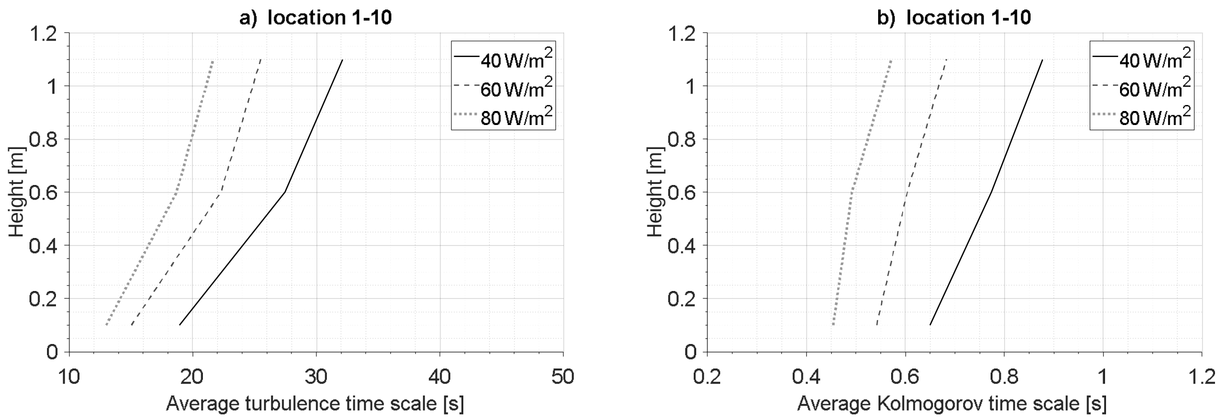

Fig. 12. The turbulence time scales at the occupied zone, case 1-3 (t_{supply}=17°C): a) large time scale, and b) small time scale.

3.10 Averaged airflow characteristics

Table 3 summarizes the test room indoor air and surrounding air conditions. The wall surface temperatures were measured at the beginning of test cases with infrared camera (Table 2). In addition, the temperature level was verified with a surface thermometer. Furthermore, the wall layer conditions were measured with data loggers during the measurements (Table 2). For instances, under common thermal load levels of 40 W/m^2 and 60 W/m^2, the diffuse ceiling surface temperature was found to range from 21-24°C and 21-28°C with the emissivity assumption of 0.96, respectively. Consequently, the temperature range seemed to increase with thermal load, most probably due to increased thermal radiation from the heat sources and due to supply airflow. In addition, the average temperature difference between the exhaust and the supply air was around 8-9°C.

Table 3. The indoor air, wall layer and surrounding air conditions.

Test cases	**40 W/m^2**	**60 W/m^2**	**80 W/m^2**
Average indoor air temperature [°C]	25.0±0.2	25.6±0.2	25.7±0.2
Indoor air temperature 0.02 m from the wall [°C]	24.6±0.5	25.3±0.5	25.5±0.5
Indoor air temperature 0.015 m from the floor [°C]	24.7±0.5	25.4±0.5	26.0±0.5
Surrounding air temperature [°C]	23.5±0.5	24.0±0.5	24.7±0.5
Average exhaust air temperature [°C]	25.0±0.2	25.8±0.2	26.0±0.2
Average supply air temperature [°C]	17.0±0.2	17.0±0.2	17.0±0.2
Supply airflow rate [l/s,m^2], floor area 21 m^2	3.6±0.1	5.2±0.1	7.3±0.1
Indoor air relative humidity [%]	40±3	35±3	44±3
Exhaust air relative humidity [%]	41±3	36±3	45±3
Surrounding air relative humidity [%]	42±3	37±3	46±3

Table 4 summarizes the mean variables of time-averaged flow field over the measured locations as a function of internal thermal load and room height. Table 4 shows the average values in the seated person zone below the height of 1.1 m in which the vertical gradient was significant. It is shown that e.g. the mean air speed was much higher near the floor at the height of 0.1 m than at the height of 0.6 m or at the height of 1.1 m with the given thermal loads. In addition, vertical difference quotients can be estimated between the highest and the lowest levels and compare the airflow characteristics interacting with the velocity field that can be used while developing indicators for thermal conditions and comfort.

Table 4. The average of variable of locations 1-10 against the internal thermal load level and room height. Column ΔQ refers to relative difference towards increasing thermal load range from 40 W/m^2 to 80 W/m^2 and column ΔH refers to a relative difference towards increasing room height from 0.1 m to 1.1 m.

Room height [m]	*0.1*	*0.6*	*1.1*	*0.1*	*0.6*	*1.1*	*0.1*	*0.6*	*1.1*	*ΔQ*	*ΔH*
Thermal load [W/m^2]	*40*	*40*	*40*	*57*	*57*	*57*	*80*	*80*	*80*	*[%]*	*[%]*
Mean air speed [m/s]	0.16	0.11	0.09	0.20	0.14	0.12	0.23	0.16	0.14	47	−40
Standard deviation [m/s] $\times10^{-2}$	6.9	6.1	5.6	7.7	7.2	6.7	8.7	8.3	7.5	32	−15
Turbulence intensity [-]	0.43	0.56	0.60	0.39	0.53	0.56	0.38	0.51	0.54	−10	42
Equivalent frequency [Hz]	0.13	0.14	0.14	0.15	0.15	0.15	0.15	0.15	0.15	9	3
Fluctuation energy [m^2/s^2] $\times10^{-3}$	4.7	3.8	3.2	6.0	5.3	4.5	7.6	6.9	5.7	73	−27
Turbulent kinetic energy [m^2/s^2] $\times10^{-3}$	2.4	1.9	1.6	3.0	2.6	2.2	3.8	3.4	2.9	73	−27
Turbulence dissipation [m^2/s^3] $\times10^{-5}$	3.9	2.7	2.2	5.5	4.6	3.6	7.9	6.8	5.2	127	−36
Large length scale [m]	2.39	0.93	0.75	2.22	1.35	1.08	2.64	1.19	0.88	16	−63
Small length scale [m] $\times10^{-3}$	3.2	3.5	3.7	2.9	3.1	3.3	2.7	2.8	3.0	−19	14
Large time scale [s]	19	27	32	15	22	26	13	19	22	−32	69
Small time scale [s]	0.65	0.77	0.88	0.54	0.60	0.68	0.45	0.49	0.57	−34	30
Large motions frequency [Hz] $\times10^{-2}$	5.3	3.7	3.1	6.7	4.5	4.0	7.7	5.4	4.7	47	−40
Small motions frequency [Hz]	1.6	1.3	1.2	1.9	1.7	1.5	2.2	2.1	1.8	51	−21
Length scale ratio [-]	754	271	207	761	452	334	1018	427	300	42	−67
Time scale ratio [-]	29	36	37	28	37	37	29	38	38	3	31
Fluctuation energy ratio [-]	0.16	0.24	0.26	0.13	0.22	0.24	0.12	0.21	0.22	−16	76

4 Discussion

The present study investigated the airflow characteristics towards increasing thermal load levels that are common in modern indoor environments. However, the airflow characteristics are only valid with diffuse ceiling ventilation and symmetrical set-up of thermal loads. The airflow interaction is different e.g. in the case of underfloor, displacement and high momentum ceiling supply air diffusers. In addition, the asymmetrical set-up of thermal loads forms a different type of flow field. Earlier studies have shown that large-scale circulating flow pattern occurs from the heat sources to the other side of the room with asymmetrical thermal load distribution that increase the temperature gradient between the perimeter and internal part [23]-[26]. Therefore, further studies can be associated with effects of asymmetric thermal load distribution on airflow characteristics.

The impact of buoyancy flows on occupied zone can be reduced most effectively by decreasing heat sources or by directing buoyancy flows into exhaust at the ceiling zone. Furthermore, a larger room height could reduce the impact, but the cooling capacity of diffuse ceiling ventilation is reduced with increased room height [41]. One system has also been a perimeter chilled beam installation using a ceiling opening and plenum cavity for the buoyancy flows, e.g. near the windows [68].

In diffuse ceiling ventilation, the vertical temperature gradient was small, i.e. 0.2°C/m, 0.3°C/m and 0.4°C/m towards increasing thermal load level of 40 W/m^2, 60 W/m^2 and 80 W/m^2, respectively. This follows the findings by Mikeska and Fan [37] and by Hviid and Svendsen [42] who also showed a small vertical temperature gradient with diffuse ceiling ventilation. Those studies also experienced highest air speed level near a floor, similarly than the current study.

Any specific frequencies were not recognized from the power spectral density function. This depicts that there is no specific peaks at the level of highest draught risk frequencies. However, the range of frequencies can be estimated from the airflow characteristics. The fluctuation energy ratio showed a relative portion of fluctuation in the flow field during the given time-interval. This condition may change with asymmetric set-up and with different air distribution method, because turbulent mixing and other flow conditions differ. The results show that the smallest length scales decrease and the largest length scales increase towards increasing thermal load. This means that the range of length scales increase with thermal load. Furthermore, this indicate logically that the airflow motions increase with thermal load. The results follow the discussion by Etheridge & Sandberg [5] and Chen and Srebric [32] who proposed that the largest scales are on the order of room size and the smallest scales from 0.01 m to 0.001 m for most indoor airflows, respectively. The supply air temperature had a small effect on the statistics of mean airflow field, although the supply airflow rate was suited to respond the change for target temperature in the occupied zone. This small effect comes obviously from the low-momentum supply airflow and the symmetrical arrangement of thermal loads.

The equivalent frequency was at a low level 0.1-0.2 Hz indicating low draught risk level, because room airflow has been shown to feel most uncomfortable when the equivalent frequency is around 0.5 Hz [15], [16]. Furthermore, the results show that the studied indoor environment could achieve the category B (*DR* 10-20 %) in the European Standard EN ISO 7730:2005 [17]. On the contrary, the results indicate that it is very difficult to provide low air-speed levels under high thermal load conditions. These results agreed the earlier study by Nielsen et al. [41] who concluded that supply airflow is not a large source of draught with diffuse ceiling ventilation.

The symmetrical set-up of thermal load and air distribution offered a good platform to investigate averaged airflow field. The diffuse ceiling ventilation enabled a low-momentum and equal supply airflow field that disturbs only a little the buoyancy driven flows from the heat sources. Overall, the airflow characteristics form a physical basis for optimizing indoor climate. When understanding better the airflow interaction, the healthy indoor environment, thermal comfort and energy efficiency can be optimized more reliable than earlier by conducting advanced HVAC-technology.

5 Conclusions

Thermal loads have an effect on thermal conditions and comfort. When thermal loads increase, the airflow motions increase, and the heat transfer increases between the individuals and surroundings. This affects the satisfaction with thermal environment. Furthermore, the results complement the earlier studies such that the buoyancy flows dominate in highly occupied indoor environments.

The supply air temperature had only a small effect on the statistics of mean air speed, although the supply airflow rate was suited to reach the target temperature in the occupied zone. This is probably due to low-momentum supply airflow from the diffuse ceiling ventilation.

The results show that the mean air speed, the standard deviation and the corresponding range mainly increase with thermal load in a time-averaged flow field of simplified thermal environment. Consequently, the airflow fluctuation increased with thermal load and with mean air speed. This reflects the airflow motions interacting with the velocity gradients and the thermal load level.

The results show that a portion of fluctuation energy was 10-30 % over the inertial energy in the seated person zone. The fluctuation energy ratio decreased slightly towards increasing thermal load levels, but increased significantly towards decreasing mean air speed levels, similarly than turbulence intensity. Furthermore, the turbulent kinetic energy and the turbulence dissipation increased with thermal load and with mean air speed.

The range of length scales increase with thermal load. The largest length-scales were on the order of the room height and the smallest length-scales were on the order of 0.001 m.

Acknowledgement

The authors wish to acknowledge L.V.Y. foundation, K. V. Lindholms foundation and Finnish Foundation for Technology Promotion (TES) for financial support and Professor Mats Sandberg from University of Gävle for discussion and comments.

REFERENCES

[1] CEN (2002). European Standard EN 13182:2002, Ventilation for buildings. Instrumentation requirements for air velocity measurements in ventilated spaces.

[2] Kosonen, R., Ahola, M., Villberg, K., & Takki, T. (2011). Perceived IEQ conditions: Why the actual percentage of dissatisfied persons is higher than standards indicate?. In Sick Building Syndrome (pp. 75-88). Springer Berlin Heidelberg.

[3] Melikov, A. K. (2016). Advanced air distribution: Improving health and comfort while reducing energy use. Indoor air, 26(1), 112-124.

[4] Tennekes H. and Lumley J. L. (1972). A First Course in Turbulence, The MIT Press, ISBN 0 262 20019 8.

[5] Etheridge, D., & Sandberg, M. (1996). Building ventilation: theory and measurement. Chichester, UK, John Wiley & Sons, ISBN 0-471-96087-X.

[6] Pope S. B. (2000). Turbulent flows, Cornell University, Cambridge University Press, ISBN 0-521-59886-9.

[7] Townsend A. A. (1976). The Structure of Turbulent Shear Flow, 2nd edition, Cambridge University Press, ISBN 0 521 29819 9.

[8] Hanzawa, H., Melikov, A.K., & Fanger, P.O. (1987). Airflow characteristics in the occupied zone of ventilated spaces. ASHRAE Transactions, vol. 93, Part 1, No. 3045.

[9] Melikov, A.K., Hanzawa, H., Fanger, P.O., 1988, Airflow characteristics in the occupied zone of heated spaces without mechanical ventilation. ASHRAE Transactions, Vol. 94, Part 1, pp.52-70.

[10] Hagström, K. (2002). Influence of kinetic energy sources and internal obstructions on room air conditioning strategy, efficiency of ventilation and room velocity conditions. Helsinki University of Technology, Department of Mechanical Engineering, Laboratory of Heating, Ventilating and Air Conditioning. ISBN 951-22-6088-3.

[11] Fanger, P. O., Melikov, A. K., Hanzawa, H., & Ring, J. (1988). Air turbulence and sensation of draught. Energy and buildings, 12(1), 21-39.

[12] Melikov, A. K., Krüger, U., Zhou, G., Madsen, T. L., & Langkilde, G. (1997). Air temperature fluctuations in rooms. Building and Environment, 32(2), 101-114

[13] Mayer, E. and Schwab, R. (1988). Direction of low turbulent airflow and thermal comfort. In: Proceedings of Healthy Buildings 88, Stockholm, Sweden, Vol.2.

[14] Toftum, J., Zhou, G., & Melikov, A. (2000). Effect of airflow direction on human perception of draught. In Proceedings of CLIMA (Vol. 2000).

[15] Zhou, G., Melikov, A. K., & Fanger P. O. (2002). Impact of equivalent frequency on the sensation of draught. Proceedings of Roomvent 2002. Copenhagen, pp. 297-300.

[16] Zhou, G., Melikov, A., 2002, Equivalent frequency - a new parameter for description of frequency characteristics of airflow fluctuations, Proceedings of Roomvent 2002, September, Copenhagen, Denmark, pp. 357-3360.

[17] CEN (2005). European Standard EN ISO 7730:2005, Ergonomics of the thermal environment — Analytical determination and interpretation of thermal comfort using calculation of the PMV and PPD indices and local thermal comfort criteria. European Standard EN ISO 7730:2005(E), 3rd edition, 2005-11-15, Geneva, Switzerland.

[18] Müller, D., Kandzia, C., Kosonen, R., Melikov, A. K., & Nielsen, P. V. (2013). Mixing Ventilation. Guide on mixing air distribution design. Federation of European Heating and Air-Conditioning Associations, REHVA, ISBN 978-2-930521-11-4.

[19] Melikov, A. K., Popiolek, Z., Silva, M. C. G., Care, I., & Sefker, T. (2007). Accuracy limitations for low-velocity measurements and draft assessment in rooms. HVAC&R Research, 13(6), 971-986.

[20] Nielsen, P. V., Restivo, A., & Whitelaw, J. H. (1979). Buoyancy-affected flows in ventilated rooms. Numerical Heat Transfer, 2(1), 115-127.

[21] Nielsen, P. V. (2011). The" Family Tree" of Air Distribution Systems. In Roomvent 2011. TAPIR Akademisk Forlag. ISBN 978-82-519-2812-0.

[22] Kosonen, R., Saarinen, P., Koskela, H., & Hole, A. (2010). Impact of heat load location and strength on air flow pattern with a passive chilled beam system. Energy and Buildings, 42(1), 34-42.

[23] Mustakallio, P., Bolashikov, Z., Kostov, K., Melikov, A., & Kosonen, R. (2016). Thermal environment in simulated offices with convective and radiant cooling systems under cooling (summer) mode of operation. Building and Environment, 100, 82-91.

[24] Bertheussen, B., Mustakallio, P., Kosonen, R., & Melikov, A. K. (2013). Comparison of the Performance of Chilled Beam with Swirl Jet and Diffuse Ceiling Air Supply: Impact of Heat Load Distribution. Clima 2013.

[25] Koskela, H., Häggblom, H., Kosonen, R., & Ruponen, M. (2012). Flow pattern and thermal comfort in office environment with active chilled beams. HVAC&R Research, 18(4), 723-736.

[26] Koskela, H., Häggblom, H., Kosonen, R., & Ruponen, M. (2010). Air distribution in office environment with asymmetric workstation layout using chilled beams. Building and Environment, 45(9), 1923-1931.

[27] Kandzia, C. (2013). Experimentelle Untersuchung der Strömungsstrukturen in einer Mischlüftung. E. ON Energy Research Center, RWTH Aachen University.

[28] Loomans, M. (1998). The measurement and simulation of indoor air flow. University of Eindhoven.

[29] Cheng, Y., & Lin, Z. (2015). Experimental study of airflow characteristics of stratum ventilation in a multi-occupant room with comparison to mixing ventilation and displacement ventilation. Indoor air, 25(6), 662-671.

[30] Zhang, Y., Liu, J., Pei, J., & Wang, C. (2017). Statistical analysis of turbulent thermal convection in a cabin mockup. Building and Environment, 115, 34-41.

[31] Wang, C., Liu, J., Li, J., Guo, Y., & Jiang, N. (2017). Turbulence characterization of instantaneous airflow in an aisle of an aircraft cabin mockup. Building and Environment, 116, 207-217.

[32] Chen, Q., & Srebric, J. (2002). A procedure for verification, validation, and reporting of indoor environment CFD analyses. HVAC&R Research, 8(2), 201-216.

[33] Zhang, C., Heiselberg, P., & Nielsen, P. V. (2014). Diffuse Ceiling Ventilation-A Review. International Journal of Ventilation, 13(1), 49-63.

[34] Zhang, C., Kristensen, M. H., Jensen, J. S., Heiselberg, P. K., Jensen, R. L., & Pomianowski, M. (2016). Parametrical analysis on the diffuse ceiling ventilation by experimental and numerical studies. Energy and Buildings, 111, 87-97.

[35] Jacobs, P., van Oeffelen, E. C., & Knoll, B. (2008). Diffuse ceiling ventilation, a new concept for healthy and productive classrooms. Proceedings of Indoor Air, paperID, 3.

[36] Fan, J., Hviid, C. A., & Yang, H. (2013). Performance analysis of a new design of office diffuse ceiling ventilation system. Energy and Buildings, 59, 73-81.

[37] Mikeska, T., & Fan, J. (2015). Full scale measurements and CFD simulations of diffuse ceiling inlet for ventilation and cooling of densely occupied rooms. Energy and Buildings, 107, 59-67.

[38] Yu, T., Heiselberg, P., Lei, B., Pomianowski, M., Zhang, C., & Jensen, R. (2015). Experimental investigation of cooling performance of a novel HVAC system combining natural ventilation with diffuse ceiling inlet and TABS. Energy and Buildings, 105, 165-177.

[39] Nielsen, P. V., & Jakubowska, E. (2009). The performance of diffuse ceiling inlet and other room air distribution systems. Cold Climate Hvac 2009.

[40] Nielsen, P. V., Jensen, R. L., & Rong, L. (2010). Diffuse ceiling inlet systems and the room air distribution. Clima 2010.

[41] Nielsen, P. V., Vilsbøll, R. W., Liu, L., & Jensen, R. L. (2015). Diffuse ceiling ventilation and the influence of room height and heat load distribution. Proceedings of Healthy Buildings Europe, Eindhoven, The Netherlands.

[42] Hviid, C. A., & Svendsen, S. (2013). Experimental study of perforated suspended ceilings as diffuse ventilation air inlets. Energy and Buildings, 56, 160-168.

[43] Saint-Gobain Ecophon (2017). Ecophon Advantage A. Internet reference: http://www.ecophon.com/en/products/Modular-ceilings/Advantage/Advantage--A/ (accessed 13.11.2017).

[44] Lindab (2017). Ventiduct VSR. Internet reference: https://itsolution.lindab.com/lindabwebproductsdoc/pdf/documentation/comfort/us/technical/vsr.pdf (accessed 13.11.2017).

[45] Zukowska, D., Melikov, A., & Popiolek, Z. (2012). Impact of geometry of a sedentary occupant simulator on the generated thermal plume: Experimental investigation. HVAC&R Research, 18(4), 795-811.

[46] CEN (2004). European Standard EN 14240:2004, Ventilation for buildings - Chilled ceilings - Testing and rating. Ref. No. EN 14240:2004: E, Brussels, Belgium.

[47] Flir (2017). ThermaCAM P60. Internet reference: http://www.flir.com/instruments/display/?id=60087 (accessed 13.11.2017).

[48] CEN (2001). European Standard EN ISO 7726:2001, Ergonomics of the thermal environment. Instruments for measuring physical quantities (ISO 7726:1998).

[49] Dantec Dynamics (2017). Vivo Draught 20T31. Internet reference: https://www.dantecdynamics.com/ (accessed 13.11.2017).

[50] Sensor Electronic (2017). SensoAnemo 5100SF. Internet reference: http://sensor-electronic.pl/ (accessed 13.11.2017).

[51] Tobin, P. (2007). PSpice for Digital Communications Engineering. Synthesis Lectures on Digital Circuits and Systems, 2(1), 1-199.

[52] Koopmans, L. H. (1995). The spectral analysis of time series. Academic press. ISBN: 978-0-12-419251-5.

[53] Gemini Data Loggers (2017). Tinytag Plus 2. Internet reference: http://www.geminidataloggers.com/data-loggers/tinytag-plus-2 (accessed 13.11.2017).

[54] FläktWoods (2017). IRIS-200. Internet reference: http://resources.flaktwoods.com/Perfion/File.aspx?id=6cc0e128-b905-4df5-b2e3-9546cadd9601 (accessed 13.11.2017).

[55] Swema (2017). Swema 3000. Internet reference: http://www.swema.com/ (accessed 9.3.2017).

[56] Ferziger, J. H., & Peric M. (2002). Computational methods for fluid dynamics. 3rd edition, Springer-Verlag. ISBN 3-540-42074-6.

[57] Wilcox, D. C. (2006). Turbulence modeling for CFD. 3rd edition, DCW industries, La Canada, California, USA, ISBN 978-1-928729-08-2.

[58] Cochran, W. T., Cooley, J. W., Favin, D. L., Helms, H. D., Kaenel, R. A., Lang, W. W., ... & Welch, P. D. (1967). What is the fast Fourier transform?. Proceedings of the IEEE, 55(10), 1664-1674.

[59] Welch, P. (1967). The use of fast Fourier transform for the estimation of power spectra: a method based on time averaging over short, modified periodograms. IEEE Transactions on audio and electroacoustics, 15(2), 70-73.

[60] MathWorks (2017a). MATLAB Documentation. Internet reference, www.mathworks.com. (accessed 13.11.2017).

[61] MathWorks (2017b). MATLAB Release Notes. Internet reference, www.mathworks.com. (accessed 13.11.2017).

[62] Kolmogorov, A. N. (1941, January). The local structure of turbulence in incompressible viscous fluid for very large Reynolds numbers. In Dokl. Akad. Nauk SSSR (Vol. 30, No. 4, pp. 301-305).

[63] Melikov, A. K., Langkilde, G., & Derbiszewski, B. (1990). Airflow characteristics in the occupied zone of rooms with displacement ventilation. ASHRAE Transactions, vol. 96, Part 1, No. 3365.

[64] Taylor, G. I. (1935, September). Statistical theory of turbulence. In Proceedings of the Royal Society of London A: Mathematical, Physical and Engineering Sciences (Vol. 151, No. 873, pp. 421-444). The Royal Society.

[65] CEN (2007). European Standard EN ISO 20988:2007 - Air quality. Guidelines for estimating measurement uncertainty (ISO 20988:2007).

[66] BIPM, IEC, IFCC, ILAC, ISO, IUPAC, IUPAP and OIML (2008). JCGM 100:2008. Evaluation of measurement data — Guide to the Expression of Uncertainty in Measurement. Évaluation des données de mesure — Guide pour l'expression de l'incertitude de mesure. GUM 1995 with minor corrections. 1st edition September 2008. Corrected version 2010. JCGM.

[67] Ratcliffe, C., & Ratcliffe, B. (2014). Doubt-Free Uncertainty in Measurement: An Introduction for Engineers and Students. Springer.

[68] Woollett, J., & Rimmer, J. (2014). Active and Passive Beam Application Design Guide. Brussels: REHVA-Federation of European Heating, Ventilation and Air Conditioning Associations.